

# FAST: An Efficient Scheduler for All-to-All GPU Communication

*Yiran Lei, Dongjoo Lee, Liangyu Zhao, Daniar Kurniawan, Chanmyeong Kim, Heetaek Jeong, Changsu Kim, Hyeonseong Choi, Liangcheng Yu, Arvind Krishnamurthy, Justine Sherry, Eriko Nurvitadhi*

## Abstract

All-to-All(v) communication is a critical primitive in modern machine learning workloads, particularly mixture-of-experts (MoE) models. Unfortunately, efficient scheduling is challenging due to workload skew, heterogeneous two-tier fabrics, and incast congestion, compounded by the dynamic nature of MoE workloads, where traffic shifts every few hundred milliseconds. Existing schedulers are hardly scalable, incurring seconds to hours of synthesis time, making them impractical.

We present FAST, an efficient All-to-All(v) scheduler. FAST addresses skew through intra-server rebalancing and enforces balanced, one-to-one scale-out transfers that avoid incast. Evaluated extensively on both NVIDIA H200 and AMD MI300X clusters, FAST consistently outperforms state-of-the-art solutions on skewed workloads while reducing synthesis time by orders of magnitude.

## 1 Introduction

All-to-All communication—where every endpoint sends data to all others—has long been a fundamental collective communication primitive in scientific and parallel computing, supporting workloads such as 3D FFTs [41]. Early systems typically treated each server as the communication endpoint, interconnected by networks with relatively uniform bandwidth. In modern ML clusters, the endpoint has shifted to individual GPUs, which are connected through a two-tier fabric consisting of faster intra-server (scale-up) links and slower inter-server (scale-out) links.<sup>1</sup> Consequently, All-to-All has become a key operation for many ML applications, including recommendation models [31, 32], Gaussian Splatting [47], and mixture-of-experts (MoE) models [14, 20, 23, 43].

The role of All-to-All in ML applications is important. In Mixture-of-Experts (MoE) models in particular, its cost can account for a large fraction of training time. MoE improves the efficiency of model parameters by activating only a subset

of experts for each input token rather than all simultaneously. This selectivity, however, necessitates frequent All-to-All operations to dispatch tokens to experts across GPUs and aggregate their outputs. Prior studies [20, 25] show that MoE All-to-All can consume 30–55% of training time, making it a major contributor to overhead in large-scale training.

The challenges of All-to-All arise at both the application and system layers. At the application layer, traffic is often **skewed** and **dynamic**. In MoE, some experts are selected more frequently than others, leading to larger data transfers for their corresponding GPUs during All-to-All. This imbalance keeps certain GPUs and NICs busy long after others have finished, creating straggler effects. When communication volumes differ across endpoints in All-to-All, the operation is referred to as `alltoallv` [30]. Further, the traffic pattern in `alltoallv` changes every few hundred milliseconds, as the MoE gating function reassigns tokens to experts at runtime (Figure 1). As a result, a GPU that is a hotspot at one moment may be nearly idle the next. This dynamism makes static `alltoallv` schedules impractical and requires schedulers to adapt in real time.

At the system layer, the hardware fabric that connects GPUs is inherently two-tiered: fast intra-server links (scale-up) and much slower inter-server links (scale-out) (Figure 4). This **heterogeneity** means that flows of the same size can finish quickly inside a server but take an order of magnitude longer across servers, leaving schedulers to coordinate thousands of flows over mismatched bandwidths. In addition, `alltoallv`'s dense communication pattern naturally triggers **incast**, a classic networking problem where many senders overload downlink of the same receiver. Incast causes network congestion with switch queue buildup and reduced goodput—even under modern congestion control—and remains an open challenge in large-scale cluster networking [12, 19].

Together, these challenges make efficient `alltoallv` scheduling especially difficult under the tight timescales demanded by MoE. Existing schedulers such as TACCL [44] and TE-CCL [27] employ solvers [18] to generate near-optimal schedules. While they overcome the inefficiencies of

<sup>1</sup>In this paper, the terms ‘scale-up’ and ‘intra-server’ network are used interchangeably, and likewise ‘scale-out’ and ‘inter-server’.

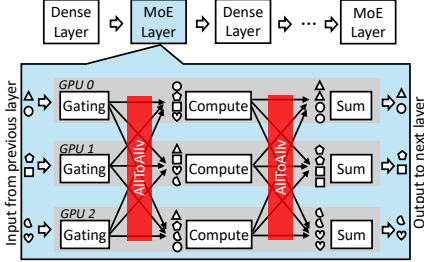


Figure 1: MoE models invoke `alltoallv` twice per MoE layer, making it a critical communication primitive.

fixed schedules in collective communication libraries such as NCCL and RCCL, their resulting formulations are NP-hard [44] and can take minutes to hours to synthesize a schedule even for just 32 GPUs. The state-of-the-art scheduler SyCCL [10] accelerates this process with heuristics and parallelism, yet require seconds to minutes for balanced All-to-All, while skewed `alltoallv` still remains unresolved. Consequently, these schedulers are far too slow for MoE `alltoallv` workloads that shift every few hundred milliseconds.

In this paper, rather than increasing scheduler complexity, we simplify the problem itself: *It suffices to focus on optimizing the scale-out tier—the real bottleneck*. We observe that scale-up is roughly an order-of-magnitude faster than scale-out (Figure 4b). So the much faster scale-up fabric can cheaply absorb skew within each server, reshaping traffic before it reaches scale-out. With this, we can then retain best possible performance by keeping bottleneck servers transmitting at full rate while avoiding incast—maximizing scale-out efficiency. This naturally reduces to a one-to-one matching problem between endpoints, solvable with polynomial-time algorithms.

Building on this insight, we propose FAST, a polynomial-time, matching-based scheduler for skewed and dynamic `alltoallv` workloads. FAST operates in two phases: (i) *Skew mitigation*, where it uses fast scale-up fabric to rebalance the scale-out workload so that all NICs face equal volume before traversing the slow scale-out links; and (ii) *Balanced, one-to-one transfers*, which use Birkhoff’s decomposition [8] to generate successive matchings between senders and receivers, ensuring scale-out transfers proceed without incast while keeping bottleneck servers fully active at line rate until completion. While Birkhoff’s decomposition has appeared in the design of crossbar switches [11, 26], this is, to our knowledge, the first application to collective communication.

We implement FAST on both NVIDIA H200 [38] and AMD MI300X [2] testbeds and evaluate it against state-of-the-art solutions such as DeepEP [46], TACCL [44], and TE-CCL [27]. Under skewed workloads, FAST outperforms the strongest NVIDIA baseline by 1.01–1.3× and the strongest AMD baselines by 1.5–2.8×, and when integrated into Megatron-LM [45] on AMD, improves end-to-end MoE training throughput by 4.48× over RCCL [5] that suffers heavily from incast. The scheduler is highly efficient, completing

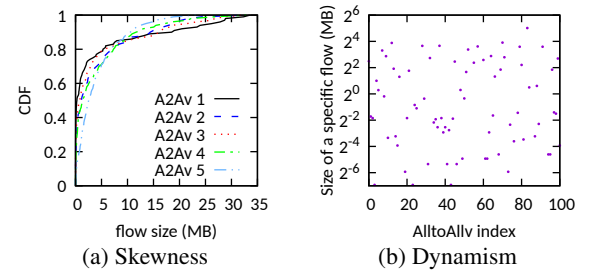


Figure 2: All-to-All workload is skewed and dynamic when using Megatron-LM to pre-train a MoE model.

in 25  $\mu$ s for 32 GPUs, 221  $\mu$ s for 64 GPUs—fast enough for MoE workloads where the traffic matrix changes every few hundred milliseconds, whereas solver-based methods require minutes to hours even at 32 GPUs. Our code will be made publicly available.

## 2 Motivation

All-to-All (`alltoallv`) communication—where every endpoint exchanges distinct data with all others—has become a key primitive in modern GPU clusters. In this setting, the communication endpoint is the individual GPU, connected by a two-tier fabric consisting of fast intra-server (scale-up) links and slower inter-server (scale-out) links.

**All-to-All communication cost in MoE models.** Mixture-of-experts (MoE) is now a leading architecture for scaling large language models: instead of activating the full model for every input, a lightweight gating network selects only a subset of ‘experts.’ This improves model parameter efficiency but requires frequent, large-scale `alltoallv` operations to dispatch tokens to their chosen experts and then gather results. As illustrated in Figure 1, each MoE layer invokes `alltoallv` twice, and MoE layers often constitute a large fraction of the model. Prior measurements [20, 25] have shown that `alltoallv` can account for 30–56% of training time.

While MoE is our primary focus, the importance of `alltoallv` extends beyond. It underpins recommendation systems [31, 32], Gaussian Splatting [47], and classical scientific workloads such as 3D FFT (where it can dominate up to 97.3% of runtime [7]!). Despite being just one collective, `alltoallv` performance disproportionately shapes the efficiency of both modern AI and traditional HPC workloads.

**Application challenges—skewness & dynamism.** To study this communication, we profile MoE training using Megatron-LM [45] with 32 experts (one per GPU). We find that `alltoallv` workloads are inherently *skewed* and *dynamical*, consistent with recent profiling results of Mixtral models [21, 25]. Unlike balanced collectives such as All-Reduce, MoE `alltoallv` generates a highly uneven demand matrix: some GPU pairs exchange more than 12× the median vol-

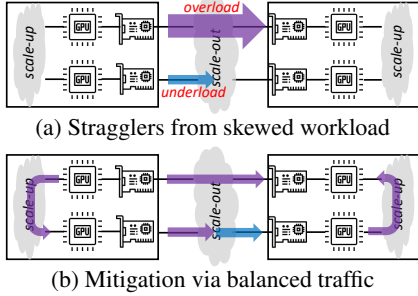


Figure 3: Workload skewness creates stragglers and underload NICs, leading to sub-optimal performance, which can be mitigated by rebalancing traffic.

ume (Figure 2a). This skew creates *stragglers*—NICs that remain busy long after others have finished, delaying the entire collective and stalling training progress (Figure 3a). In this setting, scheduling is critical: by routing part of a heavy GPU’s traffic to idle NICs, a smart scheduler can smooth out skew and mitigate stragglers, as illustrated in Figure 3b.

The MoE workload is also inherently *dynamic*: the `alltoallv` traffic pattern shifts every few hundred milliseconds. As illustrated in Figure 2b, a GPU that is *overloaded* in one `alltoallv` may become *nearly idle* in the next, since token routing is determined jointly by the input tokens and the per-MoE-layer gating functions (Figure 1). Because these patterns cannot be predicted in advance, schedules must be recomputed online at the same frequency as workload changes—making *fast, on-the-fly scheduling* essential.

**System challenges—heterogeneity & incast.** Modern GPU clusters further complicate scheduling with two system-level challenges. First, a *heterogeneous, two-tier fabric* connects GPUs (Figure 4a): fast intra-server links (e.g., NVLink, up to 900 GBps) and much slower inter-server links (e.g., InfiniBand, 400–800 Gbps). This two-tier network increases scheduling complexity: for each `alltoallv`, schedulers must navigate thousands of flows across mismatched bandwidths, exploring a large space of routing and pacing decisions, which can quickly turn scheduling itself into a bottleneck.

Second, *incast* is a classic networking problem that arises from `alltoallv`’s dense communication pattern, where many flows converge on the same NIC downlink in the scale-out fabric. While the burstiness of small messages can be absorbed by switch queues, MoE `alltoallv` transfers are much larger—typically 100 MB to 1 GB [46]—causing sustained congestion that requires active control. Even with advanced schemes [17, 19, 29], incast often results in unfair bandwidth sharing and degraded goodput. It remains an open challenge [12], and schedulers often attempt to mitigate it proactively rather than relying on the transport layer alone.

**Limitations of existing approaches.** State-of-the-art sched-

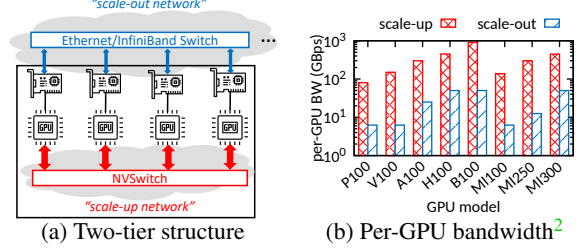


Figure 4: Modern GPU clusters feature a two-tier fabric: a high-bandwidth server/rack-scale scale-up network (e.g., NVLink, Infinity Fabric) and a lower-bandwidth cross-server scale-out network (e.g., Ethernet, InfiniBand).

ulers such as TACCL [44], TE-CCL [27], and SyCCL [10] are designed to be *general*: they support a wide range of collectives (All-Reduce, All-Gather, All-to-All, etc.) and reason about arbitrary topologies. To achieve this generality, they cast scheduling as constraint-satisfaction or optimization problems, often NP-hard [44], and solve them with heavy computation. This is practical for collectives with repetitive communication patterns like All-Reduce, where the high scheduling cost can be amortized over many iterations.

For `alltoallv`, however, existing approaches are far too slow. SyCCL [10], the fastest to date with parallelism and heuristic acceleration, is orders of magnitude faster than earlier solver-based systems but still requires minutes to produce a schedule for 64 GPUs—impractical when MoE traffic shifts every few hundred milliseconds. While such systems excel at achieving near-optimal completion under arbitrary topologies, their fine-grained modeling makes them hardly scalable to this setting.

At the other extreme, production libraries like NCCL [3] and MPI [33] generate schedules instantly, but rely on fixed schedules oblivious to the dynamic, skew workload, often resulting in much lower throughput than what the hardware could achieve.

**Goal.** Can we design a fast, online scheduler for dynamic, skewed `alltoallv` that mitigates stragglers and sustains high performance? Rather than targeting all collectives or arbitrary topologies, our goal is a *specialized* solution for `alltoallv` on today’s two-tier GPU clusters—where existing schedulers struggle to handle the underlying skewness, dynamism, asymmetry, and incast challenges.

### 3 Design Overview

To build a fast, on-the-fly scheduler for `alltoallv` in modern GPU clusters, we take a step back. Rather than enumerating complex constraints, we start by first solving `alltoallv` on a simplified single-tier network and then generalize the solution step by step to today’s asymmetric two-tier fabrics.

**Starting point: `alltoallv` in a single-tier network.** On a single-tier, full-bisection network where all links have iden-

<sup>2</sup>Bandwidth values represent full-duplex capacity (i.e., each GPU can simultaneously send and receive at the stated rate).

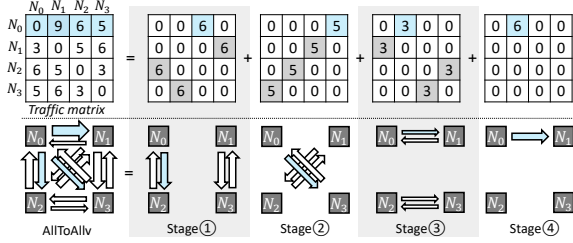


Figure 5: Birkhoff’s decomposition of a 4-node All-to-All. Completion time is dictated by the largest sender ( $N_0$  in blue), and the schedule is optimal since  $N_0$  stays active in every stage while lighter nodes drop out early.

tical bandwidth, the goal is clear: avoid incast and congestion by ensuring that, at any given time, each sender communicates with exactly one receiver, and each receiver accepts data from exactly one sender. This naturally leads to a staged schedule: in each stage, senders and receivers are matched one-to-one, and across stages, all data is exchanged across every sender–receiver combination.

For such a schedule to reach the theoretical minimum completion time, two conditions must hold: (i) each stage is balanced so all active nodes start and finish together, and (ii) the bottleneck endpoints (the heaviest senders or receivers) remain fully active at line rate until completion.

To solve this problem, we observe that Birkhoff’s decomposition [8]—introduced in 1946 as a purely mathematical identity—can be reinterpreted as an optimal scheduling strategy for `alltoallv`. Formally, the theorem states that any traffic matrix<sup>3</sup> can be expressed as a weighted sum of *permutation matrices*. Viewed through the scheduling lens, each permutation corresponds to a transfer stage: every active row (sender) and column (receiver) has exactly one nonzero entry of equal size (transfer size), so each participant exchanges data with exactly one partner and all finish the stage together. By summing over these permutation matrices, all flows advance in proportion to their demand, driving the transfer to completion.

Figure 5 illustrates our strawman approach: the top pane shows the decomposition into (partial) permutation matrices, while the bottom pane shows the corresponding transfer schedule. This approach is appealing because (i) completion time matches the lower bound—the bottleneck node (e.g.,  $N_0$  as sender in blue) transmits in *all* stages; (ii) each stage is balanced until nodes finish, so participants advance to the next stage together; and (iii) the decomposition is computationally efficient.

**Challenges of applying Birkhoff’s decomposition to heterogeneous two-tier networks.** Unfortunately, today’s GPU clusters deviate from the simplified network setting in two ways: (i) In a two-tier fabric, even a ‘balanced’ permutation

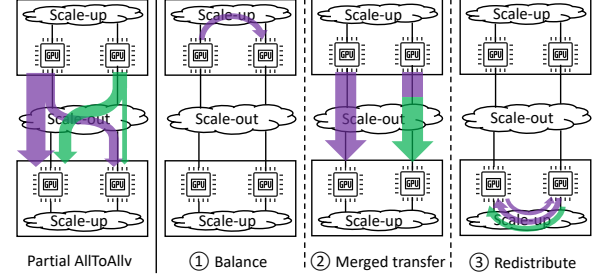


Figure 6: FAST: transforming an `alltoallv` workload with sender/receiver stragglers into a balanced scale-out transfer.

stage can finish unevenly: transfers on the slow scale-out links lag behind, idling the faster scale-up links and wasting bandwidth; (ii) More critically, completion time is dictated by the busiest scale-out NIC: the heaviest sender or receiver. If skew is large, Birkhoff’s schedule still stalls at those endpoints.<sup>4</sup>

**Our approach.** We exploit the two-tier fabric as an opportunity to simplify scheduling. Since intra-server (scale-up) bandwidth is far higher than inter-server (scale-out), it is rarely a bottleneck. We instead repurpose it to *reshape traffic in advance*, absorbing imbalance locally so the scale-out tier sees a more uniform workload and Birkhoff’s decomposition can produce more efficient schedules.

At the heart of this reshaping is another simple yet powerful observation: *what matters is delivering data to the right servers*. Which GPU inside a server handles the transfer is secondary, since intra-server shuffles are cheap compared to scale-out communication. This leads to a two-phase design:

*Intra-server scheduling: balancing and redistribution* (§4.1). Within each server, we equalize traffic across GPUs before it leaves the node (Figure 6): overloaded GPUs hand off excess traffic to lighter ones so every NIC carries the same volume per destination server. On the receiving side, each GPU receives data from exactly one designated sender on each source server, equalizing incoming volume. This process makes some data initially arrive at a ‘proxy’ GPU at the correct destination server, which is then quickly forwarded to the true destination GPU via a cheap intra-server redistribution.

*Inter-server scheduling: balanced one-to-one transfers* (§4.2). Once intra-server skew is absorbed, the remaining challenges are server-level imbalance and incast. Here, we apply Birkhoff’s decomposition to construct successive one-to-one, balanced server-to-server transfer stages, ensuring bottleneck servers remain continuously active at line rate until their traffic is complete.

Finally, we integrate these two phases into a pipelined execution that overlaps inter- and intra-server transfers (§4.3), and conclude with key properties of our scheduler, including optimality and complexity (§4.4).

<sup>3</sup>The theorem applies to scaled doubly stochastic matrices; arbitrary matrices can be adapted, as described later.

<sup>4</sup>Intra-server traffic rarely dominates in multi-node ML workloads, since the number of scale-out pairs is far larger than scale-up pairs.

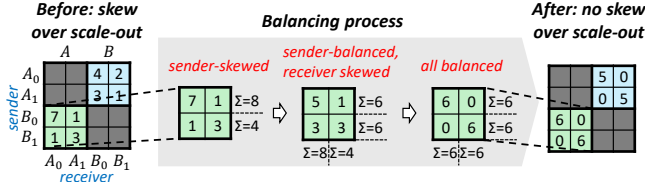


Figure 7: Balancing process for a 2-server, 2-GPU-per-server alltoallv: a skewed tile (left) is reshaped into a scalar form (right), ensuring no GPU NIC is overloaded. Grey tiles (intra-server) omitted for clarity.

## 4 Two Phase Scheduler

This section details how FAST mitigates GPU-level skew within each server through intra-server rebalancing (§4.1); addresses inter-server skew and incast by generating balanced, one-to-one transfer stages (§4.2); and integrates these mechanisms into a pipeline that overlaps intra- and inter-server traffic to optimize end-to-end performance (§4.3). We conclude by analyzing FAST’s key properties in §4.4.

### 4.1 Intra-server Scheduling: Balancing and Redistributing

The first challenge arises within each server: GPUs often generate or absorb uneven volumes of traffic, creating stragglers where some NICs sit idle while others are overloaded. By leveraging the ultra-fast scale-up fabric, our goal is to eliminate these sender- and receiver-side imbalances, presenting the scale-out tier with a more uniform workload (Figure 6).

**Example setup.** Consider a simple 2-server case ( $A, B$ ), each with 2 GPUs ( $A_0, A_1, B_0, B_1$ ). The workload is represented by a  $4 \times 4$  GPU-to-GPU traffic matrix (Figure 7). Each *row sum* reflects a GPU’s total outgoing volume; each *column sum* reflects its total incoming volume. Cross-server transfers appear as  $2 \times 2$  tiles (blue for  $A \rightarrow B$ , green for  $B \rightarrow A$ ). Since scale-out is the bottleneck, we focus on these tiles, omitting the grey intra-server diagonals for the purpose of illustration.

**Mitigating sender skew.** The first step is to prevent a GPU from being the ‘slow sender.’ In the  $B \rightarrow A$  tile, GPU  $B_0$  must send 8 units, while  $B_1$  only 4. If transmitted directly,  $B_1$  would finish early, leaving  $B_0$  as a straggler. To avoid this, we rebalance within server  $B$ : heavily loaded GPUs shift part of their traffic to lightly loaded ones using the scale-up fabric. Here,  $B_0$  transfers 2 units to  $B_1$ , so both end up with 6. In matrix terms, the *row sums* of the tile are equalized—ensuring every NIC in  $B$  contributes the same total outgoing load to server  $A$ .

**Mitigating receiver skew.** After sender-side balancing, GPU  $A_0$  may still receive 8 units (column sum) while  $A_1$  only 4, leaving a receiver-side straggler. The fix is to decouple the notions of ‘correct server’ and ‘correct GPU.’ Each sender forwards *all* of its traffic to its peer GPU with the same lo-

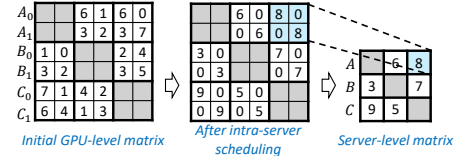


Figure 8: Intra-server scheduling reduces the initial  $6 \times 6$  GPU-level matrix ( $A_0, A_1, B_0, B_1, C_0, C_1$ ) to  $3 \times 3$  server-level matrix ( $A, B, C$ ).

cal index ( $B_0 \rightarrow A_0, B_1 \rightarrow A_1$ ), ensuring data first arrives at the correct server. This *merged peer transfer* keeps receiver loads balanced—since senders were equalized earlier—even though some data arrives temporarily at the wrong GPU, to be corrected later. In matrix form, each row collapses into a single nonzero in its peer column, turning the  $2 \times 2$  tile into a *scalar matrix* with equal diagonal entries and all off-diagonals zero (right in Figure 7). The result is one-to-one, balanced scale-out transfers across GPUs.

**Redistribution.** At this point, all traffic reaches the correct *server*, but may still be at the *wrong GPU*. A final redistribution step corrects placement inside the server, routing traffic from the proxy GPU to the true destination over the scale-up fabric. Because scale-up is an order of magnitude faster than scale-out, this added step incurs small overhead.

By combining sender balancing, merged peer transfers, and local redistribution, our scheduler reshapes *each cross-server tile* into its most balanced *scalar form*. This transformation removes intra-server skew and equalizes scale-out traffic at GPU level. What remains is the higher-level server-to-server skew, which we address next.

### 4.2 Inter-server Scheduling: Balanced, One-to-one Transfers

Although intra-server scheduling reshapes the initial skewed GPU-level All-to-All into a more balanced form, balancing over scale-up network *within each server* cannot eliminate *server-to-server* skew. Some servers still send or receive more traffic than others, creating bottlenecks that must be addressed to achieve good end-to-end performance.

This imbalance becomes clearer once we reduce the GPU-to-GPU traffic matrix into a simpler server-to-server view. Figure 8 shows a 3-server, 2-GPU-per-server example: the original  $6 \times 6$  GPU matrix (left) is reshaped by intra-server scheduling into the balanced form (middle), where each  $2 \times 2$  server-to-server tile becomes a scalar matrix. Each scalar tile can then be collapsed into a single entry, yielding the reduced  $3 \times 3$  server-level matrix (right). The intuition is that, after intra-server scheduling, GPUs within a server *act identically over scale-out*—each sending and receiving equal volumes—so we can abstract away individual GPUs. This reduction both exposes the remaining skew across servers and simplifies scheduling, since the server-level problem is typi-

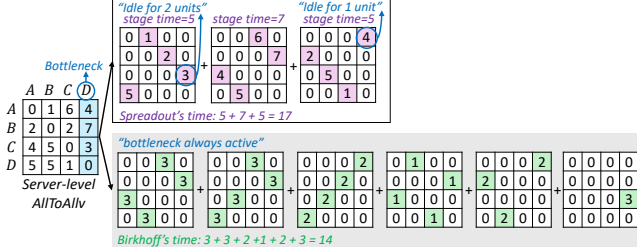


Figure 9: SpreadOut vs. Birkhoff. Both enforce one-to-one mappings, but SpreadOut (up) stalls on the largest flow in each stage, while Birkhoff (bottom) keeps bottleneck server active until completion (optimal).

cally an order of magnitude smaller than the GPU-level one (e.g., 8 GPUs per server in modern clusters).

At this server level, two scheduling challenges remain: (i) incast: even with peer access, GPU<sub>j</sub> from multiple servers may funnel into GPU<sub>j</sub> of the same destination server, overloading its scale-out link; and (ii) throughput optimality: the busiest servers must remain fully active at line rate until their traffic flows complete, otherwise the overall completion time lags behind the achievable minimum.

**SpreadOut: one-to-one but not optimal.** A natural incast-free baseline is MPI’s SpreadOut algorithm [33], which cycles through ‘shifted diagonals’ of the  $N \times N$  server matrix: at stage  $i$ , server  $s$  sends to server  $(s+i)\%N$ . This guarantees one-to-one sender-receiver mappings at every stage.

However, SpreadOut fails the second requirement: the bottleneck server may sit idle during many stages. Although the bottleneck is the row or column with the largest *sum*, its per-stage assignment may not be the largest entry on that diagonal. When this happens, the stage is gated by another flow elsewhere, forcing the true bottleneck to wait.

Figure 9 shows an example: server  $D$ , *as a receiver* is the bottleneck—with 14 units column sum—the heaviest among all rows/columns. But in stage 1,  $D$  receives only 3 units, while the stage is gated by a separate 5-unit flow ( $D \rightarrow A$  where  $D$  acts *as a sender*). As a result,  $D$  sits idle *as a receiver* for 2 extra time units. The same situation recurs in stage 3, adding another 1 unit of idle time. Altogether, SpreadOut finishes in 17 units—3 units slower than the 14-unit theoretical minimum.

In matrix terms, SpreadOut’s completion time equals the *sum of the maximum entry on each diagonal*. This sum is provably no smaller than the largest row or column sum—the true lower bound—so SpreadOut can not guarantee optimality.

**Birkhoff’s decomposition: one-to-one with optimality.** The optimal completion time is determined by the busiest server—the largest row or column sum in the matrix. In Figure 9, the busiest server  $D$  must receive 14 units, so the minimum possible time is 14. Hitting this bound requires  $D$  to receive at line rate in every stage.

Birkhoff’s decomposition [8] is tailored to this setting. It

expresses any traffic matrix<sup>5</sup> as a weighted sum of *permutation matrices*. Each permutation matrix has exactly one nonzero per row and column, all of identical value, representing a one-to-one, balanced transfer stage: every active sender transmits the same amount to exactly one receiver, and each receiver accepts from one sender. Some permutation matrices may be *partial*, with entire rows or columns set to zero, corresponding to servers that have already finished. In Figure 9, the first four stages are full permutation matrices, while the last two are partial.

Viewed as a schedule, this decomposition yields a sequence of one-to-one server-receiver matchings where bottleneck servers remain continuously active until they complete. In our example, Birkhoff finishes in 14 units—exactly the lower bound—achieving optimality.

**Multi-server end-to-end scheduling.** The final piece of our scheduler—Birkhoff’s decomposition—addresses the remaining server-level skew. We illustrate the full scheduling process with a 3-server, 2-GPU-per-server example in Figure 10, omitting intra-server transfers (grey diagonal tiles) for clarity. The input is a  $6 \times 6$  GPU-to-GPU traffic matrix (left). If GPUs transmit directly without our scheduler, the completion time lower bound is 10 time units, dictated by the heaviest sender GPU ( $B_1$ , row sum 10) and busiest receiver GPU ( $B_0$ , column sum 10).

**Step 1: Balancing.** This step reduces the severity of the bottleneck. Within each  $2 \times 2$  tile (e.g.,  $A \rightarrow B$ ), sender loads are equalized across GPUs, and *peer transfer* ( $A_i \rightarrow B_i$ ) ensures receivers share the load evenly. With intra-server skew removed, *the effective lower bound improves*: in the reshaped matrix (middle of Figure 10), the maximum row/column sum drops from 10 to 8 ( $A, C$  as sender and  $B$  as receiver). Intuitively, the pressure of a straggling NIC/GPU is averaged across all GPUs and NICs within a server, reducing its impact. At this point, the  $6 \times 6$  GPU-level matrix can be cleanly collapsed into a skewed  $3 \times 3$  server-level *alltoallv*.

**Step 2: Balanced, one-to-one transfer stages.** Birkhoff’s decomposition then partitions this server-level matrix into three balanced, one-to-one transfer stages (right). Each stage delivers a portion of the workload, and together they complete all transfers. The resulting schedule satisfies three key properties: (i) *Incast-free*: At the server level, Birkhoff enforces one-to-one matchings. Combined with Step 1’s peer-access rule, each GPU communicates *only with the same-index GPU in the matched server*, preventing any receiver overload. (ii) *Balanced*: Servers send equal volumes per stage, while Step 1 guarantees balanced GPUs within each server. (iii) *Optimal*: Bottleneck servers (e.g.,  $A, C$  as senders  $B$  as receiver here) remain fully active across all stages, achieving the theoretical minimum completion time (8 units).

**Step 3: Per-stage redistribution.** Step 2’s scale-out trans-

<sup>5</sup>Formally, the theorem applies to scaled doubly stochastic matrices; arbitrary matrices can be adapted as described later.

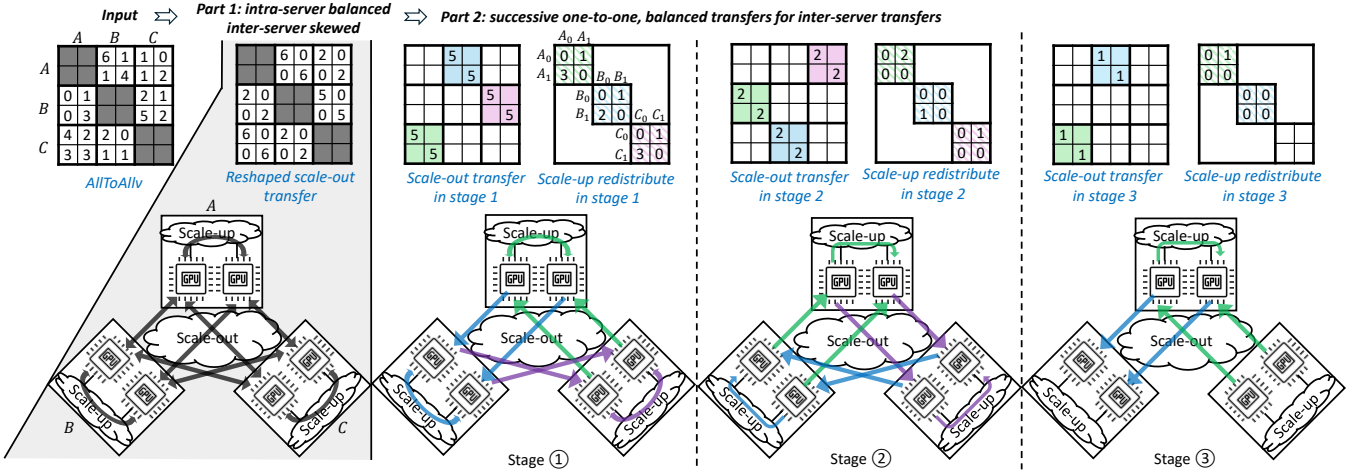


Figure 10: End-to-end scheduling example for a 3-server, 2-GPU-per-server (6x6) `alltoallv` workload. The traffic matrix (top) and transfer process (bottom) show how intra-server scheduling mitigates skew, reshaping each tile into a scalar form (left). Inter-server scheduling then applies Birkhoff’s decomposition to schedule successive one-to-one server transfers (right). Each stage is balanced, one-to-one, and keeps bottleneck servers active, achieving optimal scale-out performance.

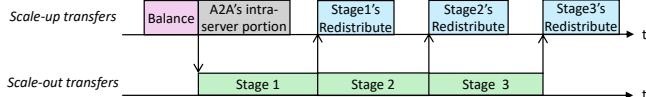


Figure 11: End-to-end transfer pipeline: scale-out transfers are kept as active as possible, while most scale-up operations are overlapped in the background. Arrows indicate triggering between steps.

fers ensure data reaches the correct server, but not necessarily the correct GPU. A lightweight redistribution step fixes placement locally, aligned with each stage. For example, in Figure 10, once  $A \rightarrow B$  (blue tile) completes in Stage 1, the corresponding portion is immediately redistributed within  $B$  (shown as the blue-striped tile).

In summary, our scheduler completes the server-level scheduling by decomposing the reshaped workload into a sequence of balanced one-to-one stages. We now turn to how these stages are executed in practice, showing how pipelining overlaps inter- and intra-server transfers to further reduce latency and hide balancing and redistribution costs.

### 4.3 End-to-End Transfer Pipeline

So far, our scheduler combines scale-up transfers (balancing and redistribution) with scale-out transfers (staged by Birkhoff’s decomposition). While scale-up is much faster than scale-out, simply *serializing everything*, e.g.,  $\text{balance} \rightarrow \text{stage 1 scale-out} \rightarrow \text{stage 1 redistribute} \rightarrow \text{stage 2 scale-out} \rightarrow \dots$ , still results in noticeable overhead. To minimize end-to-end completion time, we build a pipeline that keeps the scale-out network—the true bottleneck—as busy as possible, while pushing scale-up operations into the background.

There are three types of scale-up transfers to consider:

(i) Balancing, which equalizes GPU loads before scale-out begins; (ii) Redistribution, which was a one-time step in intra-server scheduling (§4.1) but is now aligned *per stage*, correcting placement as each stage’s scale-out completes (striped submatrices in Figure 10); and (iii) Intra-server portion of `alltoallv` (grey diagonal tiles in Figure 10). The scale-out portion is straightforward: successive one-to-one stages from Birkhoff’s decomposition.

**Pipeline structure.** Figure 11 illustrates how the pipeline operates. Balancing (purple) runs first, as all subsequent scale-out stages depend on the reshaped workload. Once balancing finishes, scale-out begins immediately. During scale-out, Stage  $i$ ’s redistribution (blue) overlaps with Stage  $(i + 1)$ ’s scale-out (green), hiding almost all redistribution cost—except in the final stage, which has no successor. The intra-server portion of `alltoallv` (grey) is executed alongside the first scale-out stage, making use of idle scale-up bandwidth before redistributions are triggered. While the pipeline could be made even tighter by subdividing balancing and scale-out into smaller chunks, the gain is marginal, so we adopt this simpler design.

Overall, the pipeline keeps the scale-out network—the true bottleneck—fully utilized, while scale-up operations are largely hidden in the background. This completes the design: intra-server scheduling removes GPU-level skew, inter-server scheduling produces balanced server-level transfers, and pipelining integrates them into a seamless end-to-end execution. Next, we turn to the key properties of our scheduler, including optimality and computational complexity.

### 4.4 Scheduler Properties

Beyond the algorithm itself, the scheduler’s properties reveal why it is a practical, efficient, and high-performance solution

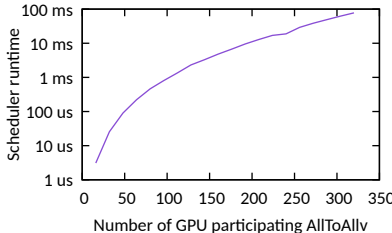


Figure 12: FAST’s scheduling runtime (with 8 GPUs per server) at scale.

for `alltoallv` in modern GPU clusters.

**Optimality.** The majority of end-to-end transfer—staged scale-out transfers generated by Birkhoff’s decomposition—operates at full efficiency on the scale-out fabric. Suboptimality arises from additional intra-server operations such as balancing and redistribution. Empirically, these costs are small: under typical workloads, they add less than 5% to the total scale-out cost (as shown in Section 5.1.3), and even under highly skewed traffic (Zipfian with skewness 0.95), the overhead remains below 8%.

We also prove in Appendix A.1 that even under adversarial workloads—designed to maximize balancing (e.g., all GPUs within a server join All-to-All but only one holds data) and redistribution (e.g., only one GPU in each destination receives data)—the performance gap from the theoretical optimum remains bounded. For instance, in a 4-node cluster with a 9:1 scale-up to scale-out bandwidth ratio (450 GBps NVLink [37] vs. 400 Gbps Ethernet), FAST finishes within 2.12 $\times$  of the optimum, even in this worst-case setting.

**Number of stages.** The number of transfer stages produced by Birkhoff’s decomposition depends on the server-level matrix. In the best case, a perfectly balanced  $N \times N$  matrix requires exactly  $N$  stages—the same as SpreadOut. With skew, more stages may be introduced, but the total is always bounded by  $(N^2 - 2N + 2)$  [22].

Fewer stages are preferable because each adds synchronization overhead. Ideally, one would minimize the stage count, but finding such a decomposition is NP-hard [15]. Rather than attempting this costly search, our scheduler efficiently produces a valid decomposition. Since the stage count is bounded, the synchronization cost is also bounded—and in practice, our evaluation shows it to be negligible.

**Computational complexity.** Intra-server scheduling is lightweight, involving only simple load balancing and redistribution bookkeeping. The main cost lies in inter-server scheduling—Birkhoff’s decomposition—which runs in polynomial time, with  $O(N^5)$  complexity. Here,  $N$  is the number of *servers*, not GPUs, since decomposition is applied only to the reduced server-level matrix.

In practice, scheduling is extremely fast on modern CPUs.<sup>6</sup>

As shown in Figure 12, our scheduler completes in 25  $\mu$ s for 4 servers (32 GPUs), 221  $\mu$ s for 8 servers (64 GPUs), and 805  $\mu$ s for 12 servers (96 GPUs), assuming 8 GPUs per server—a common configuration. With one expert per GPU, this covers the typical expert parallelism (EP) range of today’s MoE workloads: from EP8–EP128 (e.g., Perplexity AI [6]) up to very large deployments like EP320 (DeepSeek [14]). Even at EP320—40 servers—the runtime is only 77 ms, well within practical bounds.

To put this in context, consider a median-scale case with EP64: each GPU transmits about 1 GB of data to others—the data exchange scale reported by prior work [25, 46]. Over a 400 Gbps network, such an All-to-All takes at least 20 ms, while scheduling adds just 221  $\mu$ s ( $\approx 1.1\%$  of total time). Our scheduling step is a small upfront ‘tax’ that yields a fully optimized plan, shortening end-to-end completion compared to unscheduled transfers.

By contrast, prior approaches [10, 27, 44] cast scheduling as NP-hard problems (e.g., MILP or multi-commodity flow) and rely on solvers [18] that run orders of magnitude slower: for a 16-GPU All-to-All, the fastest solver-based scheduler, SyCCL, takes 3.6 s—while our scheduler runs in 3.1  $\mu$ s.

**Adaptation of an arbitrary input matrix to a valid form.** In theory, Birkhoff’s theorem applies to *scaled doubly stochastic matrices*, where *every row and column sum* is equal. Since real server matrices are arbitrary, we first embed them into this form by constructing an auxiliary matrix (always possible in  $O(N^2)$ ). The procedure increases *only the lighter rows or columns* until all sums match the heaviest one, leaving the bottleneck row/column unchanged.

This step is purely mathematical: the auxiliary entries represent ‘virtual’ transfers that are never executed. In practice, once all real traffic has finished, the auxiliary load is ignored. This is why some permutation matrices produced by the decomposition appear *partial* (Figure 9): rows or columns of all zeros stem from the auxiliary matrix. *Importantly, this conversion preserves both correctness and optimality, as the true bottleneck—the largest row or column sum—remains unchanged.*

**Exclusion of All-to-All scheduling over scale-up.** Both balancing and redistribution are themselves skewed `alltoallv` operations. Because they run entirely on the high-bandwidth scale-up fabric, sophisticated scheduling is unnecessary. For these steps we use MPI’s SpreadOut algorithm [33], which provides simple one-to-one sender–receiver mappings at low cost. While Birkhoff’s decomposition could deliver an optimal schedule here as well, its added computation is unnecessary—the scale-up tier is not the bottleneck, so the performance difference is negligible.

Another caveat is that SpreadOut may not be well suited for older GPUs with non-symmetric scale-up topologies, such as the ring in AMD MI250 [1] or the hybrid cube mesh in NVIDIA V100 [36]. However, recent GPUs adopt mostly

<sup>6</sup>Figure 12 measured on Intel Xeon Platinum 8468.

symmetric intra-server configurations, e.g., the switch-based topology [37] and the fully connected mesh [2], for scale-up fabric, which are our primary target platforms.

## 5 Evaluation

We evaluate FAST to answer four key questions:

- How does FAST compare to state-of-the-art schedulers on workloads, transfer sizes, and degrees of skew (§5.1)?
- What end-to-end throughput gains does FAST deliver to MoE training (§5.2)?
- How does FAST’s scheduling runtime compare with solver-based solutions (§5.3)?
- How does FAST scale to larger clusters and varying network bandwidths (§5.4)?

**Testbed.** We deploy FAST on two clusters with GPU Direct RDMA [4]: (i) *NVIDIA cluster*: 4 servers with NVIDIA H200 GPUs [38], each with 8 GPUs and 8 NICs, connected via 400 Gbps InfiniBand with credit-based flow control [35] and 4 KB MTU. Intra-server scale-up uses NVLink via NVSwitch, with a 9:1 scale-up to scale-out bandwidth ratio (450 GBps vs. 50 GBps). The scheduler runs on Intel Xeon Platinum 8468 CPUs. (ii) *AMD cluster*: 4 servers with AMD MI300X GPUs [2], each with 8 GPUs and 8 ConnectX-6 NICs, connected via 100 Gbps RoCEv2 Ethernet with out-of-the-box DCQCN as congestion control and 1 KB MTU. Intra-server scale-up is a fully connected Infinity Fabric mesh, with a 35:1 bandwidth ratio (448 GBps vs. 12.5 GBps). The scheduler runs on AMD EPYC 9534 CPUs.

**Libraries & dependencies.** We provide a unified Python API, `all_to_all_FAST`, mirroring PyTorch’s `all_to_all_single` for seamless integration into existing models. Implementation details differ by hardware: (i) On H200, scale-up uses CUDA IPC [34] and scale-out uses NVSHMEM [39]. (ii) On MI300X, both scale-up and scale-out are implemented with RCCL [5]. The transfer pipeline is realized with multiple CUDA/HIP streams and careful cross-stream synchronization.

**Integration into MoE systems.** FAST operates in a *distributed* fashion due to computational determinism: given the same traffic matrix, each GPU’s control thread independently computes the identical global schedule, removing the need for a central coordinator. Only the traffic matrix (a compact integer array) must be synchronized—not the schedule itself.

This integration is seamless in Megatron-LM [45], where GPUs already construct the traffic matrix before every `alltoallv`. FAST simply consumes this existing matrix, does the scheduling, and executes the transfers.

**Workloads.** We evaluate FAST on both synthetic and real MoE workloads. For synthetic workloads, we model skewness by varying GPU-pair transfer sizes using two distributions:

- (i) *random* `alltoallv` with uniformly-distributed sizes, and
- (ii) *skewed* `alltoallv` with Zipfian-distributed sizes. For real workloads, we focus on MoE training, where prior work identifies `alltoallv` as the primary bottleneck [20, 23, 25], and report the end-to-end throughput improvements achieved by FAST.

We also evaluate *repetitive, balanced* All-to-All workloads, where existing schedulers can amortize their cost, enabling fair comparison in settings favoring prior approaches.

**Metrics.** Our primary metric is *algorithmic bandwidth*, widely used in prior work [3, 44]. It captures how fast a transfer completes, defined as  $\frac{\text{Total transfer size}}{\# \text{ of GPUs} \times \text{Completion Time}}$ . Because skewed `alltoallv` may have variable per-GPU volumes, this average normalizes across all GPUs. Algorithmic bandwidth can exceed the raw scale-out link bandwidth, since part of the transfer completes locally over the faster scale-up fabric. For example, in a 4-node cluster with 50 GBps scale-out links, if 25% of the traffic is intra-server, the optimal algorithmic bandwidth is  $50/0.75 = 66.6$  GBps.

Our second metric is *scheduling runtime*, which captures the time to synthesize a schedule. Lower is better.

**Baselines.** We compare FAST against two classes of baselines: (i) *Solver-based schedulers*: TACCL [44] and TE-CCL [27], which used constraint-based solvers for scheduling. We evaluate them on both NVIDIA and AMD clusters. (ii) *Industry libraries*: On NVIDIA: NCCL [3] (recent version 2.27.3), DeepEP [46] (from DeepSeek [14]), and MSCCL [13]. On AMD: RCCL [5], SpreadOut [42] (abbreviated as ‘SPO’), and MSCCL.

Since DeepEP is NVIDIA-only, we cannot test it on AMD. NCCL is highly optimized and outperforms SpreadOut, so we omit SpreadOut results on NVIDIA. By contrast, RCCL’s `alltoallv` on AMD lacks scheduling (all flows launch concurrently), making SpreadOut a stronger baseline that we include explicitly.

### 5.1 `alltoallv` Performance

#### 5.1.1 Performance Under Different Transfer Sizes

FAST consistently achieves the best `alltoallv` performance on both NVIDIA and AMD testbeds. For baselines, NCCL, DeepEP, SpreadOut, and RCCL support `alltoallv` natively, while TACCL, TE-CCL, and MSCCL only support balanced All-to-All. Adapting the solvers to skewed `alltoallv` can be done in two ways: (i) explicitly encoding variable flow sizes into the problem formulation, or (ii) padding all flows to a uniform size so the solver sees a balanced workload (padding data is used only for scheduling, not for actual transfers). We attempted the first approach, but it made the solvers—already slow on balanced workloads (e.g., TACCL needs over 30 minutes for 32 GPUs)—incapable of finishing within a reasonable time. Thus, we adopt the padding method to simplify workloads for solver-based schedulers.

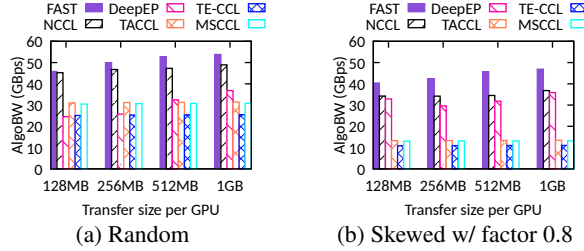


Figure 13: `alltoallv` performance on NVIDIA testbed (with 450 GBps scale-up and 50 GBps scale-out).

We evaluate with per-GPU message sizes from 100 MB to 1 GB, representative of typical workloads reported by prior work [25, 46]. The improvement factors vary across testbeds, reflecting differences in both network hardware and software implementation, as discussed below.

**Result on NVIDIA testbed.** As shown in Figure 13a, FAST achieves the highest algorithmic bandwidth under random workloads. It slightly outperforms NCCL by 1.01–1.1 $\times$ , and exceeds DeepEP (1.0–1.4 $\times$ ) and TACCL (1.5–1.7 $\times$ ). Performance generally improves with larger transfers, as scale-out links saturate more easily and staging overheads—especially in FAST—are amortized.

NCCL with PNX [28] is highly optimized: data is aggregated at the source server before being forwarded across scale-out links. While NCCL does not explicitly rebalance like FAST, PNX aggregation smooths skew in lightly skewed workloads. As a result, NCCL comes close to FAST under this workload despite lacking explicit skew handling.

DeepEP offers separate implementations for dispatch and combine `alltoallv`, both with similar performance. However, its design routes all tokens through proxy GPUs at the source server via scale-up, which under skew creates hotspots on certain proxies and their scale-up links, reducing throughput (as confirmed by DeepEP’s own NVLink profiling).

Solver-based schedulers (TACCL, TE-CCL) reconstruct skewed `alltoallv` into balanced All-to-All via padding. Although this allows near-optimal schedules in theory, padded traffic does not contribute to real transfers and delays actual data. In practice, their schedules achieve only about half of FAST’s throughput.

Straggler effects intensify under skew. With Zipfian workloads (Figure 13b), FAST outperforms NCCL by 1.2–1.3 $\times$ , DeepEP by 1.15–1.4 $\times$ , and TACCL by over 3 $\times$ . The gap with NCCL widens under medium to high skew: even after PNX aggregation, residual imbalance produces stragglers that limit NCCL’s efficiency.

**Results on AMD Testbed.** FAST again achieves the best performance under random workloads (Figure 14a), surpassing TACCL by 1.3–1.8 $\times$ , TE-CCL by 1.6–2.3 $\times$ , SpreadOut by 1.9–2.1 $\times$ , and RCCL by 1.1–10 $\times$ . As with NVIDIA, most algorithms benefit from larger transfers.

RCCL, however, shows the opposite trend: throughput de-

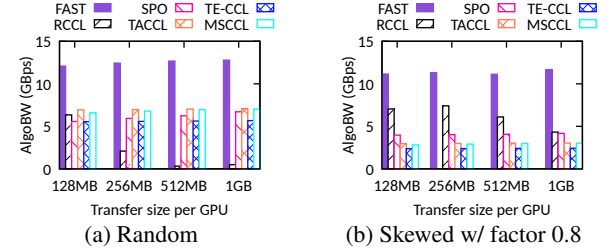


Figure 14: `alltoallv` performance on AMD testbed (with 448 GBps scale-up and 12.5 GBps scale-out).

creases with transfer size. This is mainly due to its `alltoallv` implementation—launching all flows concurrently with no scheduling—causing severe incast and reduced goodput.

Under skewed workloads (Figure 14b), FAST extends its lead, outperforming TACCL by 2.9–3.8 $\times$ , TE-CCL by 3.6–4.7 $\times$ , SpreadOut by 2.5–2.8 $\times$ , and RCCL by 1.3–2.6 $\times$ . Interestingly, RCCL performs relatively better here than under random workloads: skew concentrates traffic into a few elephant flows while leaving most as short mice transfers, reducing widespread collisions and easing incast pressure.

### 5.1.2 Performance under Balanced All-to-All

On the simple, repetitive balanced workload, DeepEP (60 GBps), TACCL (59 GBps), and NCCL (58 GBps) all achieve good performance. In this setting, FAST achieves 58 GBps—slightly below the best—since its balancing and redistribution add minor overhead unnecessary when the workload is already balanced. While prior work efficiently handles balanced All-to-All, they lack mechanisms to address skew-induced stragglers, where FAST provides clear advantages.

### 5.1.3 Performance under Different Skewness

We generate skewed workloads using a Zipfian distribution with varying skewness factors. A larger factor produces more mice flows and amplifies elephant flows, creating a stronger imbalance. The `alltoallv` traces we profile during MoE pretraining show skewness factors between 0.4 and 0.8.

On the AMD testbed, we compare FAST with TACCL, SpreadOut, and RCCL across different skewness levels (Figure 15a). FAST consistently delivers the best performance, outperforming RCCL by 1.6–10 $\times$ , SpreadOut by 2.1–3.1 $\times$ , and TACCL by 2.1–4.5 $\times$  (TE-CCL omitted here as it performs slightly worse than TACCL).

The performance gap reflects how each system handles stragglers: (i) For FAST, stronger skew increases the data that must be rebalanced, lengthening the balancing phase. As shown in the breakdown of Figure 15b, balancing time grows with skewness but remains modest: even at factor 0.9, balancing plus redistribution accounts for under 8% of scale-out time (and under 5% in most cases). Because scale-out dominates and runs at full efficiency, FAST stays within 1.05 $\times$

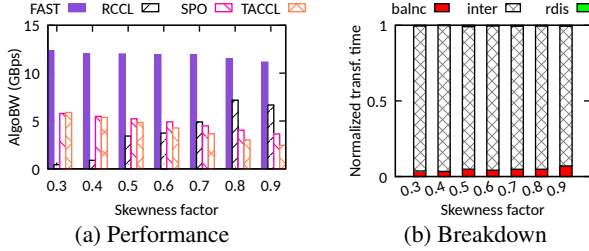


Figure 15: `alltoallv` performance and transfer time breakdown under different skewness on AMD testbed.

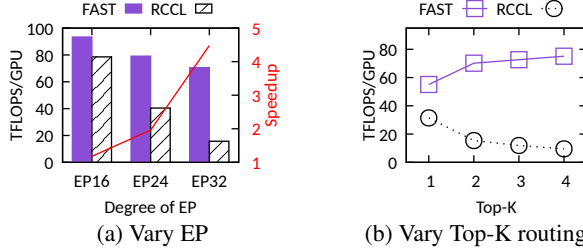


Figure 16: Megatron-LM MoE training performance improvement on AMD testbed.

of the optimal time on this AMD testbed. (ii) TACCL relies on padding, so heavier skew requires more padding, lowering effective efficiency. (iii) SpreadOut suffers as skew enlarges disparity across flows within each stage, causing stage time—and thus overall transfer time—to be dominated by stragglers. (iv) RCCL exhibits the opposite trend: higher skew generates more mice flows, which are easily absorbed by switch buffers. This reduces incast severity on the AMD testbed, improving RCCL’s performance.

## 5.2 End-to-End Performance

To evaluate FAST in an end-to-end setting, we integrate it into Megatron-LM [45] on the AMD testbed to perform on-the-fly scheduling for every `alltoallv` communication during MoE training. We compare against PyTorch’s [40] default `all_to_all_single` operator, which uses RCCL as the backend. Solver-based approaches cannot be integrated due to their prohibitive scheduling overhead.

We vary two key MoE configurations to study how FAST behaves under different training scenarios: (i) *Expert parallelism (EP)*: We sweep EP from 16 to 24 to 32, which directly determines the scale of `alltoallv`. Under the configuration where each GPU hosts one expert (like DeepSeek [14]), this corresponds to scaling the transfer from 16 GPUs (2 servers) to 32 GPUs (4 servers). (ii) *Top-K routing*: In MoE, each input token is routed to the Top-K most relevant experts; larger  $K$  increases token replication and thus flow size in the `alltoallv` workload. For this experiment, we fix EP at 32 and vary  $K$ . Other workload-related parameters, such as batch size, sequence length, and data type, similarly affect communication size and thus training performance.

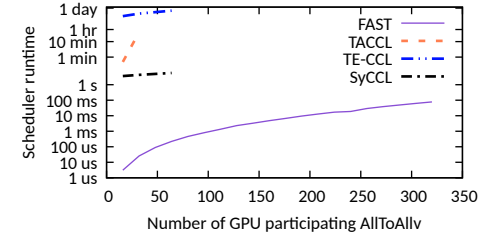


Figure 17: Comparison of FAST’s scheduling runtime against state-of-the-art solver-based schedulers (log-scale).

As shown in Figure 16a, FAST delivers a  $1.18\text{--}4.48 \times$  speedup in end-to-end training throughput (under Top-2 routing) across different EP levels. Two main trends emerge: (i) Training throughput (left y-axis) decreases as EP increases. This is expected since higher EP involves more GPUs, more servers, and thus more scale-out traffic, which lowers communication efficiency and increases GPU idle time in Megatron-LM. (ii) The baseline degrades sharply as EP grows due to escalating incast. RCCL performs no scheduling across transfers, leaving congestion entirely to the network layer. For example, with EP16, a receiver GPU/NIC handles up to 8 concurrent flows, while with EP32 this rises to 24. With only out-of-the-box DCQCN as congestion control, this causes severe throughput collapse.

As shown in Figure 16b, FAST outperforms the baseline by  $1.75\text{--}7.88 \times$  across different Top-K routing policies. Notably, FAST and RCCL follow opposite trends: (i) With FAST, increasing  $K$  enlarges flow sizes in the `alltoallv` workload, which helps amortize staging overhead and more readily saturates link bandwidth, thereby boosting throughput (consistent with Figure 14). (ii) With RCCL, however, larger  $K$  exacerbates flow collisions and congestion, leading to further degradation in communication efficiency.

## 5.3 Scheduling Overhead

FAST introduces two types of overhead relative to non-scheduling algorithms such as NCCL: (i) additional scheduling runtime, and (ii) extra memory for intermediate buffers.

**Scheduling runtime.** As shown in Figure 17, FAST scales to 320 GPUs with only 77 ms of overhead—faster than SyCCL, the fastest solver-based scheduler, which already takes 3.6 s at just 16 GPUs. In contrast, earlier solver-based methods generally fail to scale beyond 64 GPUs, rendering them unusable for moderate expert-parallelism levels such as EP96 or EP128 [6].

Even at smaller scales, their scheduling time remains prohibitively long—ranging from seconds to hours—far exceeding the transfer time itself and much longer than the interval before the workload itself changes. In comparison, FAST’s lightweight scheduling enables *on-the-fly* planning.

**Memory overhead.** FAST also requires additional memory

for temporary buffers that hold rebalanced or redistributed data. Under random workloads, this overhead is about  $\approx 30\%$  of the original `alltoallv` buffer size. In practice, the impact is minimal: typical `alltoallv` buffers are under 1 GB (e.g., in DeepEP [46]), so the extra cost is less than 300 MB. On modern GPUs such as the NVIDIA H200 [38] with 141 GB of memory, this represents under 0.22% of total capacity—an acceptable tradeoff for the performance gains.

## 5.4 Simulation at Larger Scales and Variable Bandwidths

We use simulation to evaluate FAST beyond the limits of our physical testbeds, exploring both larger scales and different scale-up/scale-out bandwidth configurations. The simulator follows the analytical framework widely used in prior work such as TE-CCL and TACCL [27, 44]: given a schedule with a sequence of transfer steps (each with a defined size), the completion time is computed by summing per-step costs. Each cost consists of a fixed link wake-up delay plus the transmission time ( $\frac{\text{data size}}{\text{link bandwidth}}$ ).

We focus on scenarios that are infeasible for solver-based schedulers, which fail to scale. Accordingly, we compare FAST against SpreadOut and an optimal bandwidth bound. This bound assumes infinitely fast scale-up links, so any intra-server transfers complete instantly. The remaining bottleneck is solely scale-out, with optimal time defined as the maximum sender or receiver load (after balancing) divided by the scale-out bandwidth.

**Performance at Larger Scale.** We first scale the number of GPUs in `alltoallv`, with each GPU pair transmitting 50 MB on average in a random workload, simulated on a 400 Gbps scale-out network and a 450 GBps scale-up network (H200). As shown in Figure 18a, FAST stays within 5% of optimal when scheduling time is excluded (“FAST raw”). Including scheduling time, the gap widens to 10% at larger scales, since scheduling cost grows faster than workload completion time (which increases only linearly with GPU count). We leave on-the-fly scheduling at extreme scale as future work. By contrast, SpreadOut achieves only about half of FAST’s throughput.

Overall performance declines as scale grows, driven by the rising share of traffic traversing the slower scale-out network.

**Performance under Varying Scale-up/Scale-out Ratios.** We also evaluate FAST under different scale-up/scale-out bandwidth ratios on a 32-GPU setup. As shown in Figure 18b, normalized bandwidth is reported relative to scale-out capacity; values can exceed 1 since about 25% of traffic is intra-server, giving an upper bound near 1.25 $\times$ . Performance improves as the scale-up/scale-out ratio increases, as faster scale-up links further reduce balancing and redistribution overhead. These results indicate that FAST sustains high efficiency on modern GPUs with advanced scale-up interconnects.

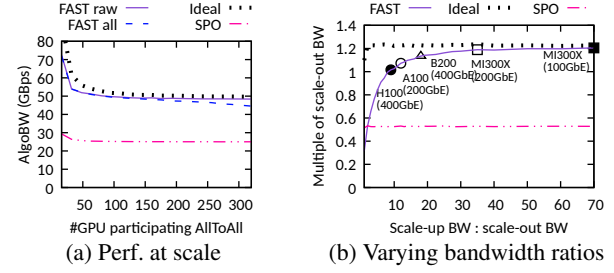


Figure 18: Simulation of FAST at larger scales and under varying scale-out/scale-up bandwidth ratios, both with random workloads.

## 6 Related Work

**Collective communication schedulers.** Classic all-to-all algorithms such as SpreadOut [33] assume a single-tier network and balanced workloads. Modern GPU libraries like NCCL [3] and RCCL [5] exploit two-tier fabrics, but they are not designed to mitigate stragglers or incast under skew. Solver-based schedulers such as SCCL, TACCL, TE-CCL, and SyCCL [9, 10, 27, 44] use SMT or MILP to generate near-optimal schedules, but are fundamentally not scalable: scheduling can take minutes to hours, making them impractical for dynamic workloads. In contrast, FAST is the first scalable, on-the-fly scheduler for skewed, dynamic `alltoallv` in modern GPU clusters.

**MoE optimizations.** Work on mixture-of-experts training [14, 16, 20, 21, 23, 24, 43] improves efficiency through model design or communication–computation overlap, but generally treats `alltoallv` as a black box. FAST complements these efforts by directly accelerating the `alltoallv` primitive itself.

**Theory-inspired designs.** Birkhoff’s theorem has also been applied to switch scheduling [11, 26]. FAST introduces a new connection, adapting Birkhoff decomposition to GPU collectives to enable efficient, polynomial-time scheduling for skewed `alltoallv`.

## 7 Conclusion

All-to-All communication is vital to modern distributed applications, especially MoE models. This paper presents FAST, the first polynomial-time, on-the-fly scheduler for skewed, dynamic All-to-All, which state-of-the-art schedulers struggle to handle. FAST exploits fast scale-up links to rebalance traffic and enforces balanced one-to-one transfers over scale-out, enabling efficient `alltoallv` communication. Evaluations on NVIDIA and AMD testbeds show that FAST outperforms state-of-the-art systems while reducing synthesis time by orders of magnitude.

*This work does not raise any ethical issues.*

## References

- [1] Amd cdna2 architecture. <https://www.amd.com/content/dam/amd/en/documents/instinct-business-docs/white-papers/amd-cdna2-white-paper.pdf>.
- [2] Amd cdna3 architecture. <https://www.amd.com/content/dam/amd/en/documents/instinct-tech-docs/white-papers/amd-cdna3-white-paper.pdf>.
- [3] Nvidia collective communications library (nccl). <https://developer.nvidia.com/nccl>.
- [4] Nvidia gpudirect. <https://developer.nvidia.com/gpudirect>.
- [5] Rocm communication collectives library (rccl). <https://github.com/ROCm/rccl>.
- [6] AI, P. Efficient and portable mixture-of-experts communication. <https://www.perplexity.ai/hub/blog/efficient-and-portable-mixture-of-experts-communication>, 2025.
- [7] AYALA, A., TOMOV, S., LUO, X., SHAEIK, H., HAIDAR, A., BOSILCA, G., AND DONGARRA, J. Impacts of multi-gpu mpi collective communications on large fft computation. In *2019 IEEE/ACM Workshop on Exascale MPI (ExaMPI)* (2019), pp. 12–18.
- [8] BIRKHOFF, G. Three observations on linear algebra. *Univ. Nac. Tucumán. Revista A.* 5 (1946), 147–151.
- [9] CAI, Z., LIU, Z., MALEKI, S., MUSUVATHI, M., MYTKOWICZ, T., NELSON, J., AND SAARIKIVI, O. Synthesizing optimal collective algorithms. In *Proceedings of the 26th ACM SIGPLAN Symposium on Principles and Practice of Parallel Programming* (Feb. 2021), ACM.
- [10] CAO, J., SHI, S., GAO, J., LIU, W., YANG, Y., XU, Y., ZHENG, Z., GUAN, Y., QIAN, K., LIU, Y., XU, M., WANG, T., WANG, N., DONG, J., FU, B., CAI, D., AND ZHAI, E. Sycl: Exploiting symmetry for efficient collective communication scheduling. In *Proceedings of the ACM SIGCOMM 2025 Conference* (New York, NY, USA, 2025), SIGCOMM '25, Association for Computing Machinery, p. 645–662.
- [11] CHANG, C.-S., CHEN, W.-J., AND HUANG, H.-Y. Birkhoff-von neumann input buffered crossbar switches. In *Proceedings IEEE INFOCOM 2000. Conference on Computer Communications. Nineteenth Annual Joint Conference of the IEEE Computer and Communications Societies (Cat. No.00CH37064)* (2000), vol. 3, pp. 1614–1623 vol.3.
- [12] CONSORTIUM, U. E. Overview of and Motivation for the Forthcoming Ultra Ethernet Consortium Specification. Tech. rep., 2023.
- [13] COWAN, M., MALEKI, S., MUSUVATHI, M., SAARIKIVI, O., AND XIONG, Y. Msclang: Microsoft collective communication language. In *Proceedings of the 28th ACM International Conference on Architectural Support for Programming Languages and Operating Systems, Volume 2* (New York, NY, USA, 2023), ASPLOS 2023, Association for Computing Machinery, p. 502–514.
- [14] DEEPSEEK-AI, LIU, A., FENG, B., XUE, B., WANG, B., WU, B., LU, C., ZHAO, C., DENG, C., ZHANG, C., RUAN, C., DAI, D., GUO, D., YANG, D., CHEN, D., JI, D., LI, E., LIN, F., DAI, F., LUO, F., HAO, G., CHEN, G., LI, G., ZHANG, H., BAO, H., XU, H., WANG, H., ZHANG, H., DING, H., XIN, H., GAO, H., LI, H., QU, H., CAI, J. L., LIANG, J., GUO, J., NI, J., LI, J., WANG, J., CHEN, J., CHEN, J., YUAN, J., QIU, J., LI, J., SONG, J., DONG, K., HU, K., GAO, K., GUAN, K., HUANG, K., YU, K., WANG, L., ZHANG, L., XU, L., XIA, L., ZHAO, L., WANG, L., ZHANG, L., LI, M., WANG, M., ZHANG, M., ZHANG, M., TANG, M., LI, M., TIAN, N., HUANG, P., WANG, P., ZHANG, P., WANG, Q., ZHU, Q., CHEN, Q., DU, Q., CHEN, R. J., JIN, R. L., GE, R., ZHANG, R., PAN, R., WANG, R., XU, R., ZHANG, R., CHEN, R., LI, S. S., LU, S., ZHOU, S., CHEN, S., WU, S., YE, S., YE, S., MA, S., WANG, S., ZHOU, S., YU, S., ZHOU, S., PAN, S., WANG, T., YUN, T., PEI, T., SUN, T., XIAO, W. L., ZENG, W., ZHAO, W., AN, W., LIU, W., LIANG, W., GAO, W., YU, W., ZHANG, W., LI, X. Q., JIN, X., WANG, X., BI, X., LIU, X., WANG, X., SHEN, X., CHEN, X., ZHANG, X., CHEN, X., NIE, X., SUN, X., WANG, X., CHENG, X., LIU, X., XIE, X., LIU, X., YU, X., SONG, X., SHAN, X., ZHOU, X., YANG, X., LI, X., SU, X., LIN, X., LI, Y. K., WANG, Y. Q., WEI, Y. X., ZHU, Y. X., ZHANG, Y., XU, Y., XU, Y., HUANG, Y., LI, Y., ZHAO, Y., SUN, Y., LI, Y., WANG, Y., YU, Y., ZHENG, Y., ZHANG, Y., SHI, Y., XIONG, Y., HE, Y., TANG, Y., PIAO, Y., WANG, Y., TAN, Y., MA, Y., LIU, Y., GUO, Y., WU, Y., OU, Y., ZHU, Y., WANG, Y., GONG, Y., ZOU, Y., HE, Y., ZHA, Y., XIONG, Y., MA, Y., YAN, Y., LUO, Y., YOU, Y., LIU, Y., ZHOU, Y., WU, Z. F., REN, Z. Z., REN, Z., SHA, Z., FU, Z., XU, Z., HUANG, Z., ZHANG, Z., XIE, Z., ZHANG, Z., HAO, Z., GOU, Z., MA, Z., YAN, Z., SHAO, Z., XU, Z., WU, Z., ZHANG, Z., LI, Z., GU, Z., ZHU, Z., LIU, Z., LI, Z., XIE, Z., SONG, Z., GAO, Z., AND PAN, Z. Deepseek-v3 technical report, 2024.
- [15] DUFOSSE, F., AND UÇAR, B. Notes on birkhoff-von neumann decomposition of doubly stochastic matrices.

*Linear Algebra and its Applications* 497 (2016), 108–115.

[16] FEDUS, W., ZOPH, B., AND SHAZER, N. Switch transformers: Scaling to trillion parameter models with simple and efficient sparsity, 2022.

[17] GAO, Y., YANG, Y., CHEN, T., ZHENG, J., MAO, B., AND CHEN, G. Dcqcn+: Taming large-scale incast congestion in rdma over ethernet networks. In *2018 IEEE 26th International Conference on Network Protocols (ICNP)* (2018), pp. 110–120.

[18] GUROBI OPTIMIZATION, LLC. Gurobi Optimizer Reference Manual, 2024.

[19] HOEFLER, T., SCHRAMM, K., SPADA, E., UNDERWOOD, K., ALEXANDER, C., ALVERSON, B., BOTTOFF, P., CAULFIELD, A., HANDLEY, M., HUANG, C., RAICIU, C., KABBANI, A., OPSASNICK, E., PAN, R., RAN, A., AND SOHAN, R. Ultra ethernet’s design principles and architectural innovations, 2025.

[20] HWANG, C., CUI, W., XIONG, Y., YANG, Z., LIU, Z., HU, H., WANG, Z., SALAS, R., JOSE, J., RAM, P., CHAU, J., CHENG, P., YANG, F., YANG, M., AND XIONG, Y. Tutel: Adaptive mixture-of-experts at scale, 2023.

[21] JIANG, A. Q., SABLAYROLLES, A., ROUX, A., MENSCH, A., SAVARY, B., BAMFORD, C., CHAPLOT, D. S., DE LAS CASAS, D., HANNA, E. B., BRESSAND, F., LENGYEL, G., BOUR, G., LAMPLE, G., LAVAUD, L. R., SAULNIER, L., LACHAUX, M.-A., STOCK, P., SUBRAMANIAN, S., YANG, S., ANTONIAK, S., SCAO, T. L., GERVET, T., LAVRIL, T., WANG, T., LACROIX, T., AND SAYED, W. E. Mixtral of experts, 2024.

[22] JOHNSON, D. M., DULMAGE, A. L., AND MENDELSOHN, N. S. On an algorithm of g. birkhoff concerning doubly stochastic matrices. *Canadian Mathematical Bulletin* 3, 3 (1960), 237–242.

[23] LEPIKHIN, D., LEE, H., XU, Y., CHEN, D., FIRAT, O., HUANG, Y., KRIKUN, M., SHAZER, N., AND CHEN, Z. Gshard: Scaling giant models with conditional computation and automatic sharding, 2020.

[24] LI, J., JIANG, Y., ZHU, Y., WANG, C., AND XU, H. Accelerating distributed MoE training and inference with lina. In *2023 USENIX Annual Technical Conference (USENIX ATC 23)* (Boston, MA, July 2023), USENIX Association, pp. 945–959.

[25] LIAO, X., SUN, Y., TIAN, H., WAN, X., JIN, Y., WANG, Z., REN, Z., HUANG, X., LI, W., TSE, K. F., ZHONG, Z., LIU, G., ZHANG, Y., YE, X., ZHANG, Y., AND CHEN, K. Mixnet: A runtime reconfigurable optical-electrical fabric for distributed mixture-of-experts training, 2025.

[26] LIU, H., MUKERJEE, M. K., LI, C., FELTMAN, N., PAPPEN, G., SAVAGE, S., SESHAN, S., VOELKER, G. M., ANDERSEN, D. G., KAMINSKY, M., PORTER, G., AND SNOEREN, A. C. Scheduling techniques for hybrid circuit/packet networks. In *Proceedings of the 11th ACM Conference on Emerging Networking Experiments and Technologies* (New York, NY, USA, 2015), CoNEXT ’15, Association for Computing Machinery.

[27] LIU, X., ARZANI, B., KAKARLA, S. K. R., ZHAO, L., LIU, V., CASTRO, M., KANDULA, S., AND MARSHALL, L. Rethinking machine learning collective communication as a multi-commodity flow problem. In *Proceedings of the ACM SIGCOMM 2024 Conference* (New York, NY, USA, 2024), ACM SIGCOMM ’24, Association for Computing Machinery, p. 16–37.

[28] MANDAKOLATHUR, K., AND JEAUGEY, S. Doubling all2all performance with nvidia collective communication library 2.12. <https://developer.nvidia.com/blog/doubling-all2all-performance-with-nvidia-collective-communication-library-2-1-2/>, 2022.

[29] MITTAL, R., LAM, V. T., DUKKIPATI, N., BLEM, E., WASSEL, H., GHOBADI, M., VAHDAT, A., WANG, Y., WETHERALL, D., AND ZATS, D. Timely: Rtt-based congestion control for the datacenter. In *Proceedings of the 2015 ACM Conference on Special Interest Group on Data Communication* (New York, NY, USA, 2015), SIGCOMM ’15, Association for Computing Machinery, p. 537–550.

[30] MPI. MPI\_Alltoallv, 2024.

[31] MUDIGERE, D., HAO, Y., HUANG, J., JIA, Z., TULLOCH, A., SRIDHARAN, S., LIU, X., OZDAL, M., NIE, J., PARK, J., LUO, L., YANG, J. A., GAO, L., IVCHENKO, D., BASANT, A., HU, Y., YANG, J., ARDESTANI, E. K., WANG, X., KOMURAVELLI, R., CHU, C.-H., YILMAZ, S., LI, H., QIAN, J., FENG, Z., MA, Y., YANG, J., WEN, E., LI, H., YANG, L., SUN, C., ZHAO, W., MELTS, D., DHULIPALA, K., KISHORE, K., GRAF, T., EISENMAN, A., MATAM, K. K., GANGIDI, A., CHEN, G. J., KRISHNAN, M., NAYAK, A., NAIR, K., MUTHIAH, B., KHORASHADI, M., BHATTACHARYA, P., LAPUKHOV, P., NAUMOV, M., MATHEWS, A., QIAO, L., SMELYANSKIY, M., JIA, B., AND RAO, V. Software-hardware co-design for fast and scalable training of deep learning recommendation models, 2023.

[32] NAUMOV, M., KIM, J., MUDIGERE, D., SRIDHARAN, S., WANG, X., ZHAO, W., YILMAZ, S., KIM, C., YUEN, H., OZDAL, M., NAIR, K., GAO, I., SU, B.-Y., YANG, J., AND SMELYANSKIY, M. Deep learning training in facebook data centers: Design of scale-up and scale-out systems, 2020.

[33] NETTERVILLE, N., FAN, K., KUMAR, S., AND GILRAY, T. A visual guide to mpi all-to-all. In *2022 IEEE 29th International Conference on High Performance Computing, Data and Analytics Workshop (HiPCW)* (2022), pp. 20–27.

[34] NICKOLLS, J., BUCK, I., GARLAND, M., AND SKADRON, K. Scalable parallel programming with cuda. In *ACM SIGGRAPH 2008 Classes* (New York, NY, USA, 2008), SIGGRAPH ’08, Association for Computing Machinery.

[35] NVIDIA. Infiniband credit-based flow control, 2005. [https://network.nvidia.com/pdf/whitepapers/deploying\\_qos\\_wp\\_10\\_19\\_2005.pdf](https://network.nvidia.com/pdf/whitepapers/deploying_qos_wp_10_19_2005.pdf).

[36] NVIDIA. Nvidia v100 gpu architecture, 2017. <https://images.nvidia.com/content/volta-architecture/pdf/volta-architecture-whitepaper.pdf>.

[37] NVIDIA. Nvidia h100 gpu architecture, 2025. <https://resources.nvidia.com/en-us-tensor-core>.

[38] NVIDIA. Nvidia h200 gpu, 2025. <https://www.nvidia.com/en-us/data-center/h200/>.

[39] NVIDIA. Nvidia openshmem library, 2025. <https://docs.nvidia.com/nvshmem/api/index.html>.

[40] PASZKE, A., GROSS, S., MASSA, F., LERER, A., BRADBURY, J., CHANAN, G., KILLEEN, T., LIN, Z., GIMELSHEIN, N., ANTIGA, L., DESMAISON, A., KÖPF, A., YANG, E., DEVITO, Z., RAISON, M., TEJANI, A., CHILAMKURTHY, S., STEINER, B., FANG, L., BAI, J., AND CHINTALA, S. Pytorch: An imperative style, high-performance deep learning library, 2019.

[41] PEKUROVSKY, D. P3dfft: A framework for parallel computations of fourier transforms in three dimensions. *SIAM Journal on Scientific Computing* 34, 4 (Jan. 2012), C192–C209.

[42] PLESIVAC-GRBOVIC, J., ANGSKUN, T., BOSILCA, G., FAGG, G., GABRIEL, E., AND DONGARRA, J. Performance analysis of mpi collective operations. In *19th IEEE International Parallel and Distributed Processing Symposium* (2005), pp. 8 pp.–.

[43] RAJBHANDARI, S., LI, C., YAO, Z., ZHANG, M., AMINABADI, R. Y., AWAN, A. A., RASLEY, J., AND HE, Y. Deepspeed-moe: Advancing mixture-of-experts inference and training to power next-generation ai scale, 2022.

[44] SHAH, A., CHIDAMBARAM, V., COWAN, M., MALEKI, S., MUSUVATHI, M., MYTKOWICZ, T., NELSON, J., SAARIKIVI, O., AND SINGH, R. Taccl: Guiding collective algorithm synthesis using communication sketches, 2022.

[45] SHOEYBI, M., PATWARY, M., PURI, R., LEGRESLEY, P., CASPER, J., AND CATANZARO, B. Megatron-lm: Training multi-billion parameter language models using model parallelism, 2020.

[46] ZHAO, C., ZHOU, S., ZHANG, L., DENG, C., XU, Z., LIU, Y., YU, K., LI, J., AND ZHAO, L. Deepep: an efficient expert-parallel communication library. <https://github.com/deepseek-ai/DeepEP>, 2025.

[47] ZHAO, H., WENG, H., LU, D., LI, A., LI, J., PANDA, A., AND XIE, S. On scaling up 3d gaussian splatting training, 2024.

## A Appendix

### A.1 Performance Bound under Adversarial Workload

We establish a theoretical bound on FAST’s performance by analyzing its behavior under adversarial workloads that trigger its worst-case execution.

We first introduce the symbols and assumptions used for proofs. There are  $n$  servers and  $m$  GPUs and  $m$  NICs within each server, making a total of  $m \times n$  GPUs participate in All-to-All. We denote the per-GPU bandwidth of scale-up and scale-out network as  $B_1$  and  $B_2$ . The scale-up network topology is a switch, while the other topology’s performance bound can be derived in a similar way. The total transfer size between two different servers  $i$  and  $j$  is denoted as  $T_{ij}$  while intra-server portion of All-to-All in server  $i$  is denoted as  $S_i$ .  $T_{ij}$  ( $i \neq j$ ) and  $S_i$  constitutes the complete All-to-All transfer workload. Note that  $T_{ii}$  does not represent anything and is thus set to be zero for the ease of writing proofs. We don’t prove the situation where the intra-node transfer is the majority of the All-to-All workload because there are more scale-out pairs than scale-up pairs in multi-node ML workload, making this scenario rare. So, we assume each server’s intra-node transfer size is no larger than the average of all the inter-node transfers, i.e.,  $S_i \leq \frac{1}{n} \sum_{j=0}^{n-1} (T_{ij})$ .

**Theorem 1.** *The optimal transfer completion time  $t_{optimal}$  is:*

$$\frac{1}{mB_2} \max\left(\max_{i=0}^{n-1} \left(\sum_{j=0}^{n-1} T_{ij}\right), \max_{j=0}^{n-1} \left(\sum_{i=0}^{n-1} T_{ij}\right)\right)$$

**PROOF.** Let us compute the transfer completion time in an ideal world where the bandwidth of an intra-node network is infinite. The intra-node transfer  $S_i$ , load balancing, and data redistribution can therefore be instantly completed. After load balancing, each GPU has  $T_{ij}/m$  amount of data waiting to be transferred via inter-server links. The inter-server transfers are bound by the largest senders or receivers among all the servers, which is  $\max(\max_{i=0}^{n-1}(\sum_{j=0}^{n-1} \frac{T_{ij}}{m}), \max_{j=0}^{n-1}(\sum_{i=0}^{n-1} \frac{T_{ij}}{m}))$ . So, the shortest transfer completion time is the value shown in the theorem. Any real-world transfers must be slower or equal to this ideal transfer.  $\square$

**Theorem 2.** FAST’s transfer worst-case completion time  $t_{FLASH}$  under the adversarial workload is:

$$\begin{aligned} t_{FAST} = & \frac{1}{mB_2} \max \left( \max_{i=0}^{n-1} \sum_{j=0}^{n-1} T_{ij}, \max_{j=0}^{n-1} \sum_{i=0}^{n-1} T_{ij} \right) \\ & + \frac{m-1}{mB_1} \max_{i=0}^{n-1} \sum_{j=0}^{n-1} T_{ij} + \frac{1}{nB_1} \max_{i=0}^{n-1} \sum_{j=0}^{n-1} T_{ij} \\ & + \frac{1}{mB_1} \max_{i,j=0}^{n-1} T_{ij}. \end{aligned} \quad (1)$$

**PROOF.** We compute FAST’s performance under adversarial workload by summing the worst-case transfer time of each transfer step: balance  $\rightarrow$  intra-server portion of All-to-All  $\rightarrow$  Birkhoff’s stages  $\rightarrow$  Final stage’s redistribution.

For load balancing, it would take the longest time to complete the job when  $T_{ij}$  is located at a single GPU in the beginning, as it causes the largest amount of data (i.e.,  $\frac{m-1}{m} \cdot T_{ij}$ ) to be balanced. For a specific server pair, it takes the source GPU  $\frac{m-1}{m} \cdot T_{ij} \cdot \frac{1}{B_1}$  amount of time to balance data. Among all the server pairs, this balancing step takes  $t_0 = \max_{i=0}^{n-1}(\sum_{j=0}^{n-1} T_{ij}) \frac{m-1}{mB_1}$ .

For the intra-server portion of All-to-All, the worst case is that all the  $S_i$  data is moved between only two GPUs, leaving the rest of the scale-up network idle. So, the worst-case time among all the servers is  $t_1 = \max_{i=0}^{n-1} \frac{S_i}{B_1} \leq \frac{1}{nB_1} \max_{i=0}^{n-1}(\sum_{j=0}^{n-1} T_{ij})$  by using the assumption  $S_i \leq \frac{1}{n} \sum_{j=0}^{n-1} (T_{ij})$ .

For staged inter-server transfer, Birkhoff’s Theorem can generate at most  $n^2 - 2n + 2$  transfer steps. We first sort them in ascending order based on each step’s transfer size and get the sorted size  $l_0 \leq l_1 \leq \dots \leq l_{n^2-2n+1}$ . We then execute the transfer steps in the sorted order, which successfully hides the current step’s data redistribution from the next step’s inter-server transfer, since (i) the redistribution time cost of stage  $i$  is  $\frac{(m-1)l_i}{B_1}$  because each GPU at destination server receives  $l_i$  amount of data from scale-out, all of which needs to be forwarded to a single GPU (worst case scenario); (ii) the scale-out transfer cost of stage  $i+1$  is  $\frac{l_{i+1}}{B_2}$ ; and (iii)  $\frac{(m-1)l_i}{B_1} < \frac{l_{i+1}}{B_2}$ , because  $l_i \leq l_{i+1}$  and  $B_1$  (e.g., 450 GBps in H100) is

more than  $(m-1) = 7$  times faster than  $B_2$  (e.g., 50 GBps) under today’s  $m = 8$  cluster. This means staged scale-out transfers from Birkhoff’s theorem are consecutive, making the actual scale-out transfer time  $t_2$  equals  $t_{optimal}$  from the ideal setting because Birkhoff let the bottleneck servers keep transmitting.

Finally, for the last stage’s redistribution, since each stage does a one-to-one server matching, the worst case is when the last stage’s scale-out transfer picks the largest transfer size among all the server pairs, which is  $\max_{i,j=0}^{n-1} T_{ij}/m$ , making the worst-case completion time as  $t_3 = \frac{1}{B_1} \max_{i,j=0}^{n-1} \frac{T_{ij}}{m}$ .

Therefore, FAST worst-case transfer time under adversarial workload is  $t_{FAST} = t_0 + t_1 + t_2 + t_3$ , which is the value shown in the theorem.  $\square$

With optimal performance and FAST’s worst-case performance, we can calculate the performance bound.

**Theorem 3.** The gap between FAST’s worst-case performance and optimal performance is bound by  $\frac{B_2}{B_1}(m + \frac{m}{n})$ .

**PROOF.** We divide FAST worst-case transfer time by ideal transfer time as follows:  $\frac{t_{FAST}}{t_{optimal}} = \frac{t_0 + t_1 + t_2 + t_3}{t_{optimal}} \leq 1 + \frac{B_2}{B_1}(m + \frac{m}{n})$  where we shrink the denominator as follows:

$$\max(\max_{i=0}^{n-1}(\sum_{j=0}^{n-1} T_{ij}), \max_{j=0}^{n-1}(\sum_{i=0}^{n-1} T_{ij})) \geq \max_{i=0}^{n-1} \sum_{j=0}^{n-1} T_{ij} \geq \max_{i,j=0}^{n-1} T_{ij}$$

to cancel out the numerator and get the final result.  $\square$

In conclusion, under adversarial workloads, the worst-case performance gap of FAST relative to optimal is bounded by the scale-up to scale-out bandwidth ratio. With today’s hardware—for example, a 4-node cluster with 450 GBps scale-up on H100 [37] and 400 Gbps scale-out—this bound implies that FAST’s worst-case scenario completes within 2.12 $\times$  of the theoretical optimum. In practice, this worst-case adversarial workload rarely happens and the performance is much closer to optimal as we show in the evaluation.